

Measurement of radiation profile at density ramp-up phase by using AXUV photodiode arrays in Heliotron J

S. Watanabe, K. Nagasaki^a, H. Matsuoka, H. Arimoto, T. Mizuuchi^a, H. Okada^a, S. Kobayashi^a, K. Kondo, S. Yamamoto^a, N. Tamura^b, C. Suzuki^b, G. Motojima, K. Murai, F. Hamagami, H. Yasuda, K. Mukai, A. Nakajima, D. Katayama, H. Takahashi and F. Sano^a

Graduate School of Energy Science, Kyoto University, Gokasho, Uji, Kyoto 611-0011, Japan

^a *Institute of Advanced Energy, Kyoto University, Gokasho, Uji, Kyoto 611-0011, Japan*

^b *National Institute for Fusion Science, 322-6 Oroshi-cho, Toki 509-5292, Japan*

(Received day month year / Accepted day month year should be centered 10-point type)

Measurement of radiation profiles has been made in electron cyclotron resonance heated (ECRH) plasmas on Heliotron J by using AXUV photodiode arrays. The measured radiation in low density is attributed to the effect of low energy photon below about 10eV at edge region, and the profile in the chord-integrated signal is found to be broad. The radiation collapse at density ramp-up is also investigated. The radiation starts to decrease from the edge side at the collapse, and then the reduction in the radiation gradually shifts to the core plasma during the collapse event. The plasma starts to collapse when the edge radiation intensity reaches a certain value, independent of the density.

Keywords: Heliotron J, radiation profile, AXUV, soft x-ray profile, radiation collapse

1. Introduction

Radiation from plasmas plays an important role in confinement and transport in toroidal devices. The radiative process is related to the impurity transport, radiation collapse, and MARFE phenomenon. The energy loss from the radiation is a key issue for high density plasma confinement in stellarators which reach higher densities than tokamaks. The physics of density limit have been investigated by several scenarios, which involve the increase in radiated power with density [1]. The observation in W7-AS and LHD suggests that the density limit is determined by the power balance between the input power and the radiative power [2, 3].

Absolute extreme ultraviolet photodiodes (AXUVD) are widely used for plasma diagnostic to understand the radiation process. The AXUVD is capable of measuring the radiation with high time resolution with energy sensitivity from visible to soft-x ray region. Some of the applications are , for example, a total radiation power monitor from visible to soft-x region with unfiltered AXUVD, a fast measurement of vacuum ultraviolet (VUV) and soft-x emission with filtered AXUVD, and a fast spectroscopic measurement of plasma impurities with AXUVD using multilayer filters [4-6]. In this paper, we present measurement results on radiation profiles by using the AXUVD for ECRH plasmas in Heliotron J. The

radiation profile in low density is shown, and the radiation collapse event at density ramp-up phase is also reported.

2. Experimental setup

Heliotron J is a medium sized helical-axis heliotron device with a low magnetic shear ($\langle R_0 \rangle = 1.2$ m, $a=0.1\text{-}0.2$ m, $B_0 < 1.5$ T). The coil system consists of an $l/m=1/4$ continuous helical coil, two sets of toroidal coils and three pairs of vertical field coil. The combination of these coil sets produces flexible helical-axis heliotron fields. The two sets of toroidal coils controls the bumpiness component of the magnetic field in Boozer coordinates, $\varepsilon_b = B(m/n=0/4)/B(m/n=0/0)$, which is an important component in the helical-axis heliotron configuration because of its contribution to neoclassical transport and improved particle confinement. For plasma heating, second-harmonic X-mode ECRH (70GHz 0.4 MW) is applied. The details of Heliotron J are described in Ref. 7.

Two AXUVD arrays (AXUV 16ELO/G, IRD) have been installed in Heliotron J in order to measure radiation profiles. One array views over the whole poloidal cross section with an optical filter system, and the other views from the plasma center to the SOL in the inboard side of torus without optical filter. The AXUVD has a high time resolution with the rise time of 0.5 μ s. The filter system at one photodiode array is composed of aluminum foils with

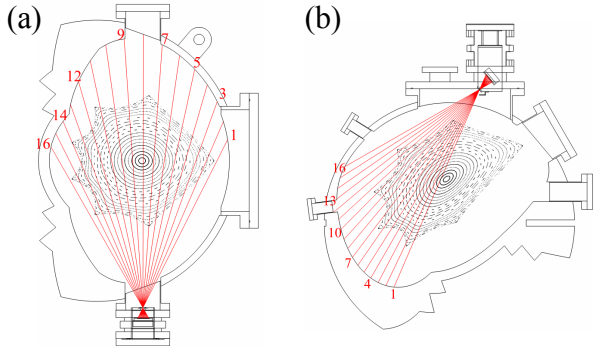


FIG. 1 Magnetic flux surface and lines of sight of AXUVD arrays
(a) viewed over the whole poloidal cross section and (b) viewed from the plasma center to the SOL in the inboard side of torus

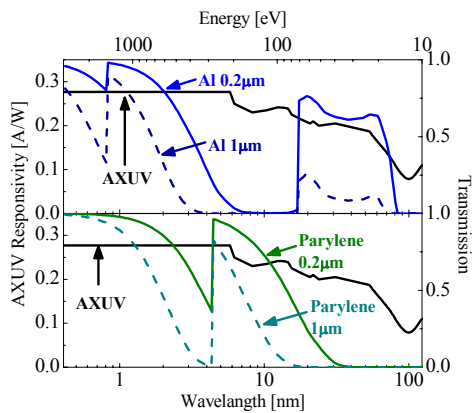


FIG. 2 AXUVD responsivity and transmission of aluminum and parylene filters

1.0 μm and 0.2 μm thicknesses, parylene foils of 1.0 μm and 0.2 μm thicknesses, and a bandpass filter for 155 nm (FWHM 26.6 nm, FN155-N-.5D-MTD-SP, ACTON). The transmission characteristics in these filters and the spectral responsivity in AXUVD are shown in Fig. 2. The aluminum foil eliminates the effect of the low energy photon and transmits the high energy photon. On the other hand, the parylene foil eliminates the photon energy from UV to VUV regions. The transmission curves in the foils are also shown in Fig. 2. The radiation in soft-X and VUV region is estimated by using combination of the aluminum and parylene foils.

3. Measurement of radiation profile

3.1 Measurement with optical filter system

The radiation profiles have been measured in low density ($\bar{n}_e \sim 0.7 \times 10^{19} \text{ m}^{-3}$) ECRH plasmas by using the AXUVD array to view over the whole poloidal cross section. Shown in Fig. 3 are the radiation profiles of the chord-integrated signals without the optical filter and with 0.2 μm aluminum and 0.2 μm parylene filters, where 8ch signal corresponds to the magnetic axis. Note that the 9 and 16ch signals are not used due to a trouble in the AXUVD array system. The radiation profile in the integrated signals without filter is rather asymmetric

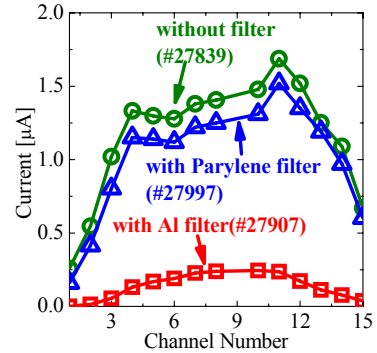


FIG. 3 Radiation profiles without the optical filter and by using 0.2 μm aluminum and 0.2 μm parylene filters

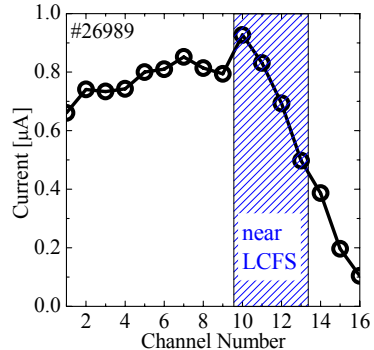


FIG. 4 Radiation profile by using AXUVD in Fig. 1(b)

which have a peak at 11ch at the inside of the torus, and resembles in shape with the parylene filter. The parylene filter of 0.2 μm thickness eliminates the energy photon below about 50 eV, but has the transmission characteristics in visible light. On the other hands, the radiation profile by using the 0.2 μm aluminum filter, which eliminates the effect of energy photon from about 80 to 200 eV and below 10 eV, is centrally peaked, and the intensity at the edge region is low. The radiation intensity with the aluminum filter is about 20% as low as without the filter. The result indicates that the radiation from low energy photons below about 10 eV dominates and causes the asymmetry in the measured radiation without filter. Shown in Fig. 4 is the radiation profile in the integrated signals without the filter by using the AXUVD illustrated in Fig. 1(b). The profile is hollow which have a peak at 10ch near the last closed flux surface (LCFS). The radiation intensity with the aluminum filter near LCFS (2, 14ch) in Fig. 1(a) is much lower than without filter. The effect of low energy photon below 10 eV should be dominant near the edge region.

3.2 Radiation profile during collapse event

In this section, the radiation profile at density ramp-up in ECRH plasmas is studied by using two AXUVD arrays. The measurement has been carried out in the plasma at more than $2 \times 10^{19} \text{ m}^{-3}$ in electron density. The typical time evolution of plasma discharge is shown in Fig. 5. The

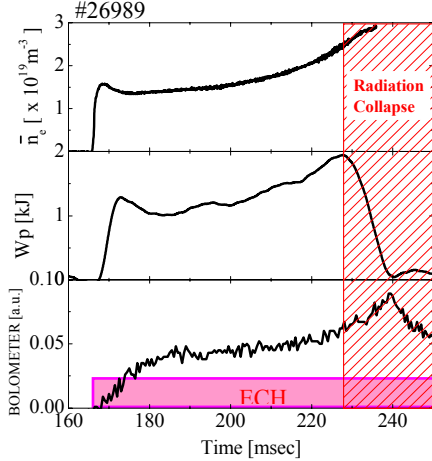


FIG. 5 Typical wave forms of a radiative collapse discharge for ECR heating plasma (shot #26989)

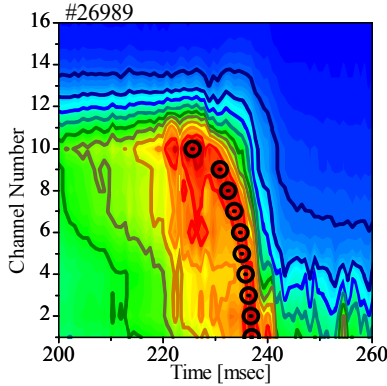


FIG. 6 Radiation profile evolution in the chord-integrated signal with radiation collapse event. The open circles indicate the maximum intensity of the signal at each channel inside 10ch during the collapse event.

bolometer signal is measured by a metal resistor type bolometer without metal foil filter [8]. The signal includes the effect of the neutral particle because no filter is applied to block off the particle. As the radiation collapse arises after 227 ms in this discharge, the stored energy decreases and the bolometer signal increases. Figure 6 shows the radiation profile in the chord-integrated signal measured by the AXUVD array in Fig. 1(b). The 10ch signal viewing near the last closed flux surface is largest and increases with density. The signal decreases suddenly with the stored energy at the collapse event. As the radiation collapse proceeds, the peak of the profile moves toward the central region. The open circles in Fig. 6 indicate the maximum intensity of the signal at each channel inside 10ch during the collapse event. The peak of the radiation profile shifts gradually from edge to core plasma after near the time for the maximum stored energy. Since no significant changes in the signals at core region (1-5ch) are observed at $t \sim 227$ ms, it can be seen that the collapse emerges from the edge region. The collapse phenomena often occurred in wall conditioning discharges in early FY2007 campaign in

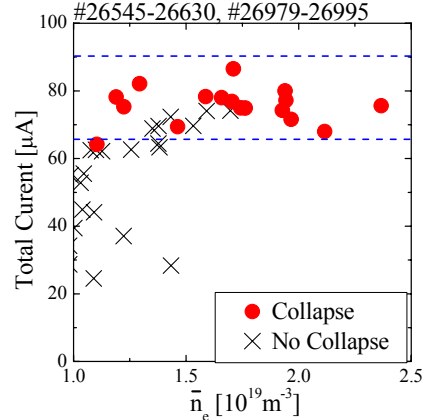


FIG. 7 Total radiation intensity just before the collapse event (collapse case) and at time for the maximum stored energy (non-collapse case) in the early experimental campaign

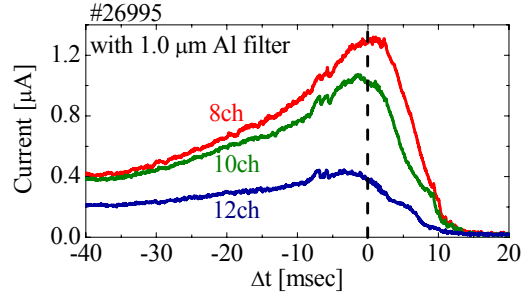


FIG. 8 Time series of radiation intensities at the collapse event by using AXUVD with 1.0 μm aluminum filter. The dashed line indicates the time for the maximum stored energy and Δt is time interval from the timing.

Heliotron J. Figure 7 shows the density dependence of the total radiation intensity. Here the total radiation is estimated by summing the intensities in all the channels at the time for the maximum stored energy. The radiation collapse occurs when the total signal current reaches between about 65 and 90 μA , independent of the electron density. Since the density is lower than the ECRH cut-off density, the collapse should be triggered by radiation loss above certain radiation intensity.

The change in radiation during the collapse event was also measured by the AXUVD array with the optical filter system shown in the Fig. 1(a). Similarly as Fig. 6, the radiation intensity without filter firstly decreases from the edge side and then the reduction region shifts to the core region at same time scale as Fig. 6. On the other hands, the measurement by the array with 1 μm aluminum filter was carry out in order to eliminate the energy photon below about 400 eV in the discharge with the collapse as shown in Fig. 8, where Δt is time interval from timing in the maximum stored energy. No clear shift of reduction region of radiation intensity by using the aluminum filter is observed during the collapse event. Figure 9 shows the time in peak (over 95% of maximum) of radiation intensity at each channel. The time in shift of

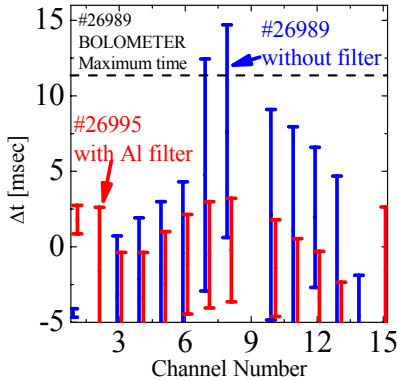


FIG. 9 Time region in the peak (over 95% of maximum) of the radiation intensity at each channel in AXUVD array

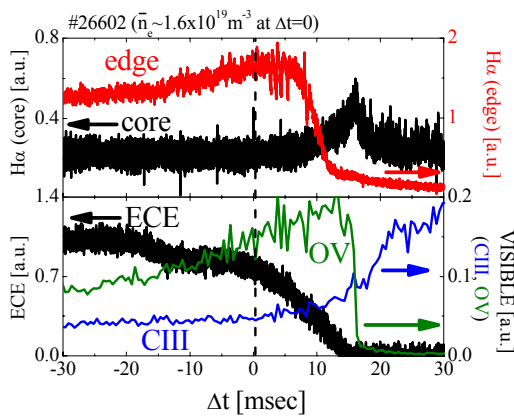


FIG. 10 Time series of the signals from $H\alpha$, OV, CIII and ECE at the collapse event

the reduction region exceeds 10 ms in non-filter case, but a few ms in the aluminum filter case. The timing at reduction of the central channel (8ch) signal in the radiation profile without filter is later than with the filter. The change in radiation profile during the collapse event should be the effect of shift of emission region from energy photon below about 400 eV. The signals of $H\alpha$ at edge and core region, OV and CIII viewed whole poloidal cross section are shown in Fig. 10. Similarly in the signals of AXUVD, the timing at reduction in $H\alpha$ signal at the core is later than at the edge, and the signal at the core is kept increasing to near $\Delta t=15$ ms. On the other hands, the OV and CIII signals increase at the collapse event, and the OV signal drops at $\Delta t \sim 15$ ms. The electron cyclotron emission (ECE) signal, shown in Fig. 10, decreases after $\Delta t=0$ ms. Since the density is lower than the ECRH cut-off density, it suggests that the electron temperature decrease during the collapse event. As the ionization potential of CIII and OV are respectively 47.9 and 114 eV, the signal drop in OV is due to cooling of the plasma. As a result of energy loss in the radiation collapse, the radiation from the energy photon below 400 eV should be dominant, and increases by reduction in the electron temperature.

4. Summary

Measurement of radiation profiles was carried out for ECRH plasmas in Heliotron J by using two AXUVD arrays. The radiation profile in the line-integrated signals is rather asymmetric, which has a peak in inside of the torus in low density plasma of $\bar{n}_e \sim 0.7 \times 10^{19} \text{ m}^{-3}$. Comparison between the radiation profiles with and without the filter showed that the radiation from low energy photons below about 10 eV dominated and caused the asymmetry. The radiation intensity near LCFS is high, and the radiation from the low energy photon was found strong at the edge region.

The radiation collapse at density ramp-up ($\bar{n}_e > 2 \times 10^{19} \text{ m}^{-3}$) was also investigated. The peak of radiation moves from the edge side during the collapse event. No significant changes in the radiation at the core region are observed just after the collapse event, and the collapse emerges from the edge region. The radiation collapse occurs when the emission intensity reaches a threshold, independent of the electron density, suggesting that the collapse should be triggered by radiation-loss above certain radiation intensity. The radiation intensity with 1 μm aluminum filter decreases at each channel near timing of maximum in the stored energy. The reduction timing for radiation without filter is later than that with the filter. The ECE signal decreases with increasing the density, and the signals from $H\alpha$ at the core, OV and CIII signals increase during the collapse. These measurement results suggest that the electron temperature decreases from the edge region, and the low temperature region spreads into the core region.

Acknowledgements

The authors are grateful to the Heliotron J team for their excellent arrangement of the experiments.

References

- [1] Greenwald M, Plasma Phys. Cont. Fusion **44** R27-80 (2002)
- [2] Giannone L et al., Plasma Phys. Cont. Fusion **42** 603 (2000)
- [3] Peterson BJ et al., Plasma Fusion Res. **1** 045 (2006)
- [4] Suzuki C et al., Rev. Sci. Insutrum. **75** 4142 (2004)
- [5] Xiao Q et al., Rev. Sci. Insutrum. **67** 3334 (1996)
- [6] Lanier NE et al., Rev. Sci. Insutrum. **72** 1188 (2001)
- [7] Obiki T. et al., Nucl. Fusion. **41** 833 (1999)
- [8] Besshou S et al., Jpn. J. Appl. Phys. **23** L839 (1984)